Available online at www.sciencedirect.com
SCIENCE DIRECT®
Biomaterials 27 (2006) 460–472
Biomaterials
www.elsevier.com/locate/biomaterials

Neurite bridging across micropatterned grooves

Joshua S. Goldner[1], Jan M. Bruder[1], Grace Li, Daniele Gazzola, Diane Hoffman-Kim*

Department of Molecular Pharmacology, Physiology, and Biotechnology and Center for Biomedical Engineering, Brown University, Providence, RI 02912, USA

Received 29 June 2005; accepted 30 June 2005
Available online 22 August 2005

Abstract

After injury, regenerating axons must navigate complex, three-dimensional (3D) microenvironments. Topographic guidance of neurite outgrowth has been demonstrated in vitro with culture substrates that contain micropatterned features on the nanometer-micron scale. In this study we report the ability of microfabricated biomaterials to support neurite extension across micropatterned grooves with feature sizes on the order of tens of microns, sizes relevant to the design of biomaterials and tissue engineering scaffolds. Neonatal rat dorsal root ganglion (DRG) neurons were cultured on grooved substrates of poly(dimethyl siloxane) coated with poly-L-lysine and laminin. Here we describe an unusual capability of a subpopulation of DRG neurons to extend neurites that spanned across the grooves, with no underlying solid support. Multiple parameters influenced the formation of bridging neurites, with the highest numbers of bridges observed under the following experimental conditions: cell density of 125,000 cells per sample, groove depth of 50 μm, groove width of 30 μm, and plateau width of 200 μm. Bridges were formed as neurites extended from a neuron in a groove, contacted adjacent plateaus, pulled the neuron up to become suspended over the groove, and the soma translocated to the plateau. These studies are of interest to understanding cytoskeletal dynamics and designing biomaterials for 3D axon guidance.

Keywords: Micropatterning; Polydimethylsiloxane; Nerve tissue engineering; Laminin

1. Introduction

Traumatic injury to the spinal cord can result in significant reduction of function and multiple complications in victims of such injuries. After injury, neurons do not spontaneously regenerate their axons, largely due to the inhibitory post-lesion environment that impedes regrowth on multiple levels. Myelin-associated molecules act to block axon growth [1–3] and the formation of an astrocytic glial scar also acts as a barrier for regeneration [4–6]. In the past few decades, advances in our comprehension of nerve regeneration have confronted previous beliefs that CNS neurons were inherently incapable of regrowth. In the 1980s Aguayo and colleagues provided injured neurons in the brain and spinal cord with peripheral nerve grafts, and demonstrated that CNS neurons retain the capacity for regrowth when provided with an appropriate, permissive environment [7,8].

After nerve injury, successful nerve regeneration requires the coordinated presentation of multiple permissive signals, many of which have been incorporated into biomaterial platforms designed to promote regrowth. Candidate axon guidance cues include diffusible factors such as neurotrophins [9], substrate-bound factors such as extracellular matrix and cell adhesion molecules [10], and electrical gradients [11]. A number of studies have drawn attention to the fact that interactions with the three-dimensional (3D) extracellular microenvironment influence neuronal growth, mediating

*Corresponding author. Tel.: +1 401 863 9395; fax: +1 401 863 1753.
E-mail address: Diane_Hoffman-Kim@brown.edu (D. Hoffman-Kim).
[1]These two authors contributed equally to this work.

0142-9612/$ - see front matter © 2005 Elsevier Ltd. All rights reserved.
doi:10.1016/j.biomaterials.2005.06.035

functions such as adhesion, migration, and neurite extension [12–15]. Thus, topography has been added to the list of factors that can influence nerve growth and regeneration.

Cellular abilities to respond to topographical features in their environments have been known for a number of years [16–18]. Surface features can direct cellular functions such as activation, orientation, and migration [17]. The observation that fibroblasts modulate their orientation and morphology in response to surface topographies gave rise to the principle of contact guidance [19,20]. The term "contact guidance" typically refers to the phenomenon where a cell encounters a geometrical feature (for example, a step) and is both inhibited from crossing over it and polarized along the length axis of the feature. The contact guidance phenomenon has been described in particular in regard to the response of cells to repeating grooved topography over a wide range of feature dimensions [21–31].

Neurite extension both during development and after an injury requires mechanical interactions between growth cone and substrate. Neurons have the capacity to respond to topographical features in their microenvironments, and they have been shown to adhere, migrate, and orient their axons to navigate surface features such as grooves in substrates [23,32–35]. For the past few decades, micropatterned substrates have been used as tools to study and direct neurite outgrowth. Initially, proteins were patterned using simple techniques that allowed the investigation of guidance effects, but lacked reproducibility and precision on the cellular level, at the physiologically relevant micron scale. With the implementation of microlithography adapted from the microelectronics industry [36,37], topographically patterned features can be transferred to polymers for use as cell culture substrates [22,38]. This versatile technology facilitates the precise and reproducible control of adhesive and topographical substrate features. Subsequently, topographic guidance of neurite outgrowth has been explored in vitro with culture substrates that contain well-defined micropatterned features on the nanometer-micron scale [25,33,35,39,40].

In this study we employed photolithographic techniques to create poly(dimethyl siloxane) (PDMS) grooved substrates with feature sizes in the range of tens to hundreds of microns. This scale is larger than that previously investigated in the context of directing neurite outgrowth. It is important to examine these features because they are critical for the design of biomaterial scaffolds and porous matrices for neural tissue engineering for spinal cord repair. Postnatal rat dorsal root ganglion (DRG) neurons were cultured on laminin-coated micropatterned substrates, and neurite outgrowth was evaluated after 24 h in culture. Here we describe an unusual neurite extension phenomenon that to our knowledge has not been reported previously. DRG neurons extended neurites that spanned across grooves of widths up to 200 μm. The neurite bridges were as long as 495 μm and were characterized by a lack of solid substrate to support the bridge region. Time-lapse microscopy analysis of bridge formation suggests that neurites can adhere to plateaus and pull a neuron into a suspended bridge position. We discuss the implications of these observations both for understanding the fundamental mechanisms of neurite outgrowth and for the design of future biomaterials that can promote directed axon growth.

2. Materials and Methods

2.1. Substrate production

2.1.1. Pattern design and printing

Patterns for photolithography were designed with AutoCAD LT 2004 (Autodesk) and printed on high resolution transparent film at 10,000 dpi (CAD/Art Services, Inc.). At this resolution, features with sizes of 3 μm were reliably reproducible.

2.1.2. Photolithography

Standard photolithography techniques were used to pattern substrates. Si wafers (Silicon Sense Inc.) were coated with a layer of negative tone Nano SU-8 50 photoresist (MicroChem) by spin coating with a CEE100 spinner (Brewer Scientific) in a two stage process: (1) spinning at 500 rpm for 10 s with a ramp of 100 rpm/s, and (2) spinning at 2000 rpm for 30 s with a ramp of 300 rpm/s. Wafers were baked at 65 °C for 6 min, 95 °C for 20 min, and slowly cooled to 22 °C. Photoresist was polymerized by UV exposure through the pattern film with a Karl Suss mask aligner (MJB3 UV300) at 5.3 mW/cm^2 for 1.1 min. Wafers were baked at 65 °C for 2 min, 95 °C for 5 min, and slowly cooled. Non-crosslinked photoresist was dissolved with SU-8 Developer (MicroChem), and wafers were rinsed with isopropanol and dried under nitrogen.

2.1.3. Preparation of poly(dimethyl siloxane) (PDMS) substrates

Tridecafluoro-1,1,2,2-tetrahydrooctyl-1-trichlorosilane (silane, United Chemical Technology) was deposited under vacuum onto the micropatterned wafers to prevent adhesion of the photoresist to the PDMS during casting. Sylgard 184 PDMS elastomer base (Dow Corning) was mixed with Sylgard 184 PDMS curing agent at a 10:1 wt/wt ratio, degassed, poured onto a micropatterned wafer to a thickness of 1–2 mm, degassed, cured at 95 °C for 45 min, and peeled off the wafers to generate substrates of 1 cm × 1 cm × 1–2 mm for cell culture. Substrates were post-baked at 95 °C for 45 min to ensure completion of the curing reaction.

All coating and cell culture reagents were from Invitrogen Life Technologies unless otherwise indicated. PDMS substrates were plasma activated at 10.5 W for 60 s with a plasma cleaner/sterilizer (PDC – 32 G, Med RF level, Harrick), sterilized by immersion in 70% ethanol, and rinsed with sterile dH_2O. Substrates were coated with 100 μg/ml poly-*L*-lysine

(PLL, 70–150 kDa, Sigma) for one hour, rinsed with dH_2O, coated with 50 μg/ml mouse laminin in Hanks' Balanced Salt Solution without calcium or magnesium (HBSS-CMF) for one hour, and rinsed with dH_2O before plating.

2.2. Cell culture

Cells were cultured as detailed below for each cell type. All cultures were incubated at 37 °C and 5% CO_2 in a humidified environment. For culture on micropatterned substrates, cells were initially plated at specified densities onto substrates in 100 μl of appropriate plating medium. After cells adhered to substrates for 3 h, 3 ml of appropriate culture media were added.

2.2.1. Dorsal root ganglion (DRG) culture

DRG were dissected from the spinal columns of postnatal (P0–P4) rat pups and cleaned of axons, blood, and connective tissue. DRG were incubated in 0.05% trypsin-EDTA in HBSS-CMF at 37 °C for 60 min and dissociated by trituration. Cells were plated at specified densities (see Results and Discussion) onto substrates in serum-containing base medium: Dulbecco's Modified Eagle's Medium (DMEM), 10% fetal bovine serum, 4 mM L-glutamine, penicillin (100 U/ml)/streptomycin (100 μg/ml) and 50 ng/ml nerve growth factor (NGF). After cells adhered to substrates, additional serum-containing media was added.

2.2.2. Hippocampal neuron culture

Hippocampi from embryonic day 18 (E18) rat pups were dissected on ice in HBSS-CMF, 1% HEPES buffer (1 M) and penicillin (100 U/ml)/ streptomycin (100 μg/ml). Hippocampi were incubated in 0.05% trypsin-EDTA at 37 °C for 15 min and dissociated by trituration. Cells were plated onto micropatterned substrates at 50,000 cells/cm^2 in Earle's Modified Eagle's Medium, 1 mM pyruvic acid, 0.6% glucose and 10% horse serum. After cells adhered to substrates, neurobasal media with 0.25% Glutamax and 2% B27 supplement was added.

2.2.3. Schwann cell culture

Schwann cells were obtained from adult rat sciatic nerve using methods described by Morrissey et al. [41]. Briefly, sciatic nerve from an adult rat was harvested and cleaned of epineurium, blood vessels and connective tissue. The sciatic nerve was cut into 1 mm^2 explant pieces that were cultured in DMEM with 10% FBS on tissue culture plastic dishes. Media was changed every 3 days, and explants were transferred to fresh dishes every 7 days for 6 weeks to allow for fibroblast migration out of the explants. Once fibroblast migration was complete, explants were digested with 0.3% trypsin-EDTA, 0.1% collagenase IV and 0.1% hyaluronidase at 37 °C for 1 h, and dissociated by trituration. Dissociated Schwann cells were cultured on dishes coated with 100 μg/ml PLL in DMEM supplemented with 10%FBS, 1% L-glutamine, 2 μM forskolin, 10 μg/ml bovine pituitary extract and penicillin (100 U/ml)/ streptomycin (100 μg/ml) (Schwann cell media). Cells at passage 20–25 were cultured on micropatterned substrates at 50,000 cells/cm^2 in Schwann cell media.

2.2.4. B104 Cell culture

Rat neuroblastoma B104 cells were cultured on micropatterned substrates at 50,000 cells/cm^2 in DMEM with 10% FBS, 4 mM L-glutamine, and penicillin (100 U/ml)/streptomycin (100μg/ml).

2.3. Fixing and immunostaining

Samples were fixed with 1% paraformaldehyde (Sigma), 2% sucrose (CalBiochem), in 0.1 M phosphate buffered saline, pH 7.4 (PBS) for 15 min at room temperature, then rinsed with PBS. Nonspecific staining was blocked by incubating for 1 h at room temperature with 10% goat serum, 1% bovine serum albumin (Sigma), in PBS (blocking buffer) with the addition of 0.1% Triton X-100 (VWR) for permeabilization. Samples were incubated overnight at 4 °C with primary antibody diluted in blocking buffer, rinsed in PBS, incubated for 1 h at room temperature with appropriate Cy3-conjugated secondary antibody (Jackson Laboratories) diluted 1:200 in blocking buffer, rinsed in PBS, and viewed under fluorescence microscopy. Primary antibodes included a polyclonal rabbit antibody directed against laminin (1:500, Biomedical Technologies Inc.), a mouse monoclonal antibody MAB079 directed against S-100 protein (1:200, Chemicon), and a mouse monoclonal antibody RT97 (1:200), that was directed against the phosphorylated epitopes of neurofilament, developed by Dr. John Wood, and obtained from the Developmental Studies Hybridoma Bank (developed under the auspices of NICHD and maintained by the University of Iowa). For controls, samples were processed without incubation with primary antibody.

2.4. Analysis

2.4.1. Confocal microscopy

Samples coated with PLL and laminin were processed for laminin immunocytochemistry as in 2.3, sectioned, and examined under confocal microscopy. Immunostained samples were embedded in Tissue-Tek OCT resin (Sakura Finetek), sections were cut at 30 μm thickness with a Leica CM 1510-3 cryostat, and sections were mounted on superfrost microscope slides (VWR) for examination on a spectral confocal microscope (Leica TCS SP2 AOBS). Slides were viewed with a 63 × oil immersion lens and *z*-plane slices of 1.11 μm per slice were obtained per section. Stacks of multiple *z*-planes were assembled using Voxx 2.0 software (University of Indiana).

2.4.2. Phase contrast and epifluorescence microscopy

Samples plated with cells were examined on a Nikon Eclipse TE2000-S microscope, equipped with phase-contrast and epifluorescence optics with appropriate filter cubes. Images were captured using a Hamamatsu Orca-ER camera and Orbit shutter controller (Improvision), outputting to OpenLab v4.0.2 (Improvision) running on Mac OS v10.3.

2.4.3. Scanning electron microscopy

For examination under scanning electron microscopy (SEM), samples were fixed in paraformaldehyde as described above, fixed further in Karnovsky's fixative for 3 h, rinsed in 0.1 M cacodylate buffer, and postfixed in 1% OsO_4 in 0.1 M

cacodylate buffer for 1 h. Samples were incubated as follows: dH_2O, 1% thiocarbohydrazide in dH2O for 30 min, dH_2O, 0.5% OsO_4 in dH_2O for 30 min, and graded ethanols to 100% ethanol. After air drying and gold–palladium coating, samples were examined with a Hitachi S-2700 SEM using an acceleration voltage of 3 kV. Image contrast was corrected to improve visibility of the neurites, using the Adobe Photoshop CS level function.

2.4.4. Quantification and statistical analysis

Numbers of bridging cellular extensions were observed under phase-contrast optics at 200x magnification and counted for each sample, with the examiner blinded to the experimental conditions. Bridges were counted in unfixed samples to eliminate the possibility of disruption of bridges by the fixation process. Ten grooves were analyzed for each sample. These representative areas were selected to be at least 500 μm from the sample edges to avoid edge effects of cell plating.

To evaluate the significance of substrate and cell conditions on neurite bridging, one-way analysis of variance was performed for each group (cell density, groove width, and plateau width) in the between-subject design (ANOVA). Post-hoc multiple comparison analysis was done using Tukey's test. SPSS 11.5 software was used, and significance levels were taken to be $p = 0.05$.

2.4.5. Time-lapse microscopy

For time-lapse microscopy, cells plated on substrates were cultured at 37 °C and 5% CO_2 in an incubation chamber with a heater and a carbon dioxide enrichment accessory (Solent Scientific). Images were collected with the Nikon microscope and Orca-ER camera system described above. Using custom-designed Openlab 4.0.2 automations, images were recorded every 5 min between 3–24 h post-plating. At each time point, 20 focal planes were recorded with 5 μm spacing between planes. Images were analyzed using Volocity 3.1 (Improvision).

3. Results and discussion

3.1. Micropatterned substrates

Micropatterned PDMS substrates contained repeating rectangular groove—plateau patterns with varied groove width (w_g), varied plateau width (w_p), and a constant groove depth (d_g) of 50 μm (Fig. 1A–C). Substrates were coated with laminin, an extracellular matrix glycoprotein that is expressed ubiquitously along pathways in the developing nervous system [42], that accelerates regeneration after injury [43–45], and that promotes neurite outgrowth in vitro [42]. Confocal microscopy confirmed that both groove and plateau regions were coated with laminin (Fig. 1D), and these substrates were used for experiments in order to vary a single feature—surface topography—in the context of a growth-promoting molecular microenvironment.

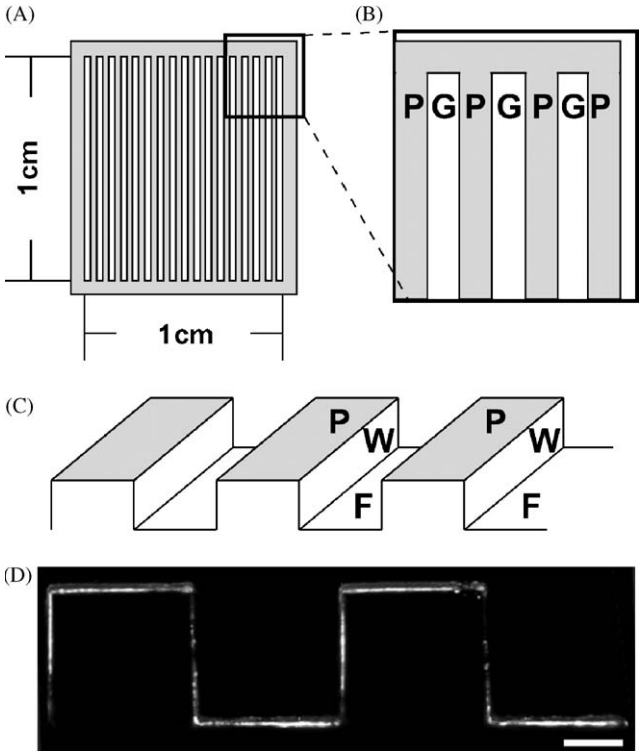

Fig. 1. Experimental design: A. Top view cartoon of micropatterned PDMS substrate with repeating groove pattern; overall surface area for cell seeding is 1 cm^2. B. Close-up top view cartoon of micropatterned PDMS substrate showing alternating topographical features: grooves (white) and plateaus (shaded). Widths of grooves and plateaus were varied in these experiments. C. Three-dimensional view cartoon of micropatterned PDMS substrate. D. Confocal z-stack of a 30 μm section of micropatterned PDMS with w_g of 60 μm and w_p of 60 μm. Substrate was coated with PLL and laminin, and stained for anti-laminin immunofluorescence. Twenty-five planes of 1.11 μm per plane were combined into a single stack. Scale bar, 25 μm. P, plateau; G, groove; W, groove wall; F, groove floor.

3.2. Bridges across micropatterned grooves

Topographical surface features of substrates can influence nerve function and in particular, show a robust impact on neurite outgrowth. There is a large body of evidence that demonstrates contact guidance of neurites along grooved topographical features at the nanometer—single micron scale. In the present study, we report that accompanying their ability to align to grooves and plateaus, postnatal rat DRG neurons have an additional capacity for a distinctly different response; neurons can extend neurites that form "bridges" spanning from one plateau to an adjacent plateau across relatively wide micropatterned grooves, with w_g on the order of tens of microns.

A "bridge" was defined as a cellular process that crossed a groove to extend between two adjacent plateaus (Figs. 2; 3A, C, D; 4). In some cases, cellular processes extended between a groove wall or floor and another groove wall or a plateau (Fig. 3B); however, for

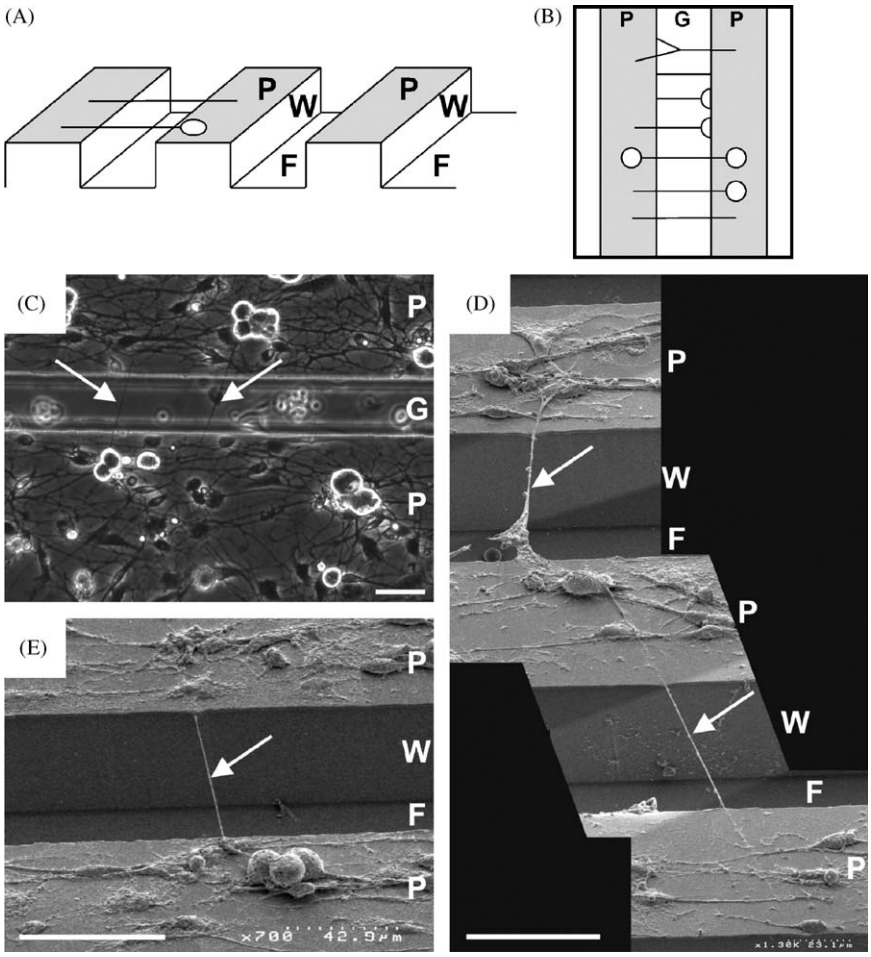

Fig. 2. DRG bridges on micropatterned substrates: A. Three-dimensional view cartoon of micropatterned PDMS substrate depicting two typical neurites spanning across the groove on the left. Circles represent somata and lines represent neurites. B. Top view cartoon of micropatterned PDMS with various configurations of bridging neurites, including those with one, two, or no soma visible on adjacent plateaus, and those with single or branching neurites. Circles represent somata and lines represent neurites. C. Phase contrast photomicrograph of DRG after 24 h culture on laminin-coated, micropatterned PDMS substrate with cell density of 125,000 cells/cm^2, w_g of 50 μm and w_p of 1 mm. Two bridging neurites are shown (arrows); each connects between a soma on a plateau and the surface of the respective adjacent plateau, spanning across the groove. D. Scanning electron micrograph of DRG after 24 h culture on laminin-coated, micropatterned PDMS substrate with cell density of 125,000 cells/cm^2, w_g of 50 μm and w_p of 70 μm. Two bridging neurites are shown (arrows); each connects between a soma on the upper plateau and the surface of the respective adjacent plateau, spanning across the groove. The bridging neurites do not interact with the groove wall or groove floor. The upper bridging neurite was originally attached to its lower plateau at two points; the left attachment region broke during processing. Multiple images were assembled with the Photomerge function in Adobe Photoshop. E. Scanning electron micrograph of DRG after 24 h culture on laminin-coated, micropatterned PDMS substrate with cell density of 125,000 cells/cm^2, w_g of 50 μm and w_p of 70 μm. A neurite (arrow) bridges between two adjacent plateaus without interacting with the groove wall or groove floor. P, plateau; G, groove; W, groove wall; F, groove floor. Scale bars, 50 μm.

the quantification portion of this study, we excluded these types of extensions from being counted as neurite bridges (see below). Bridging extensions were immunopositive for neurofilament, confirming that they were neurites (Fig. 4). Bridges exhibited diverse morphologies, as demonstrated under both phase-contrast microscopy and SEM. In some cases a bridge was composed of a single neurite (Figs. 2, 3D, 4) or multiple neurites, while in other instances, cell somata as well as neurites were components of the bridge (Fig. 3A, C). Bridges extended at various angles, with observed lengths up to 495 μm.

3.3. Conditions for neurite bridges

In the present study, DRG neurons exhibited neurite bridges on micropatterned substrates with the following features: d_g of 50 μm, w_g of 30–100 μm, and w_p of 30–1000 μm. Multiple parameters correlated with the numbers of neurite bridges. For the purpose of quantifying numbers of neurite bridges and correlating these numbers with substrate parameters, we applied a narrow definition of ''neurite bridge'' as a cellular process that extended between two adjacent plateaus and exhibited a morphology of the types shown in

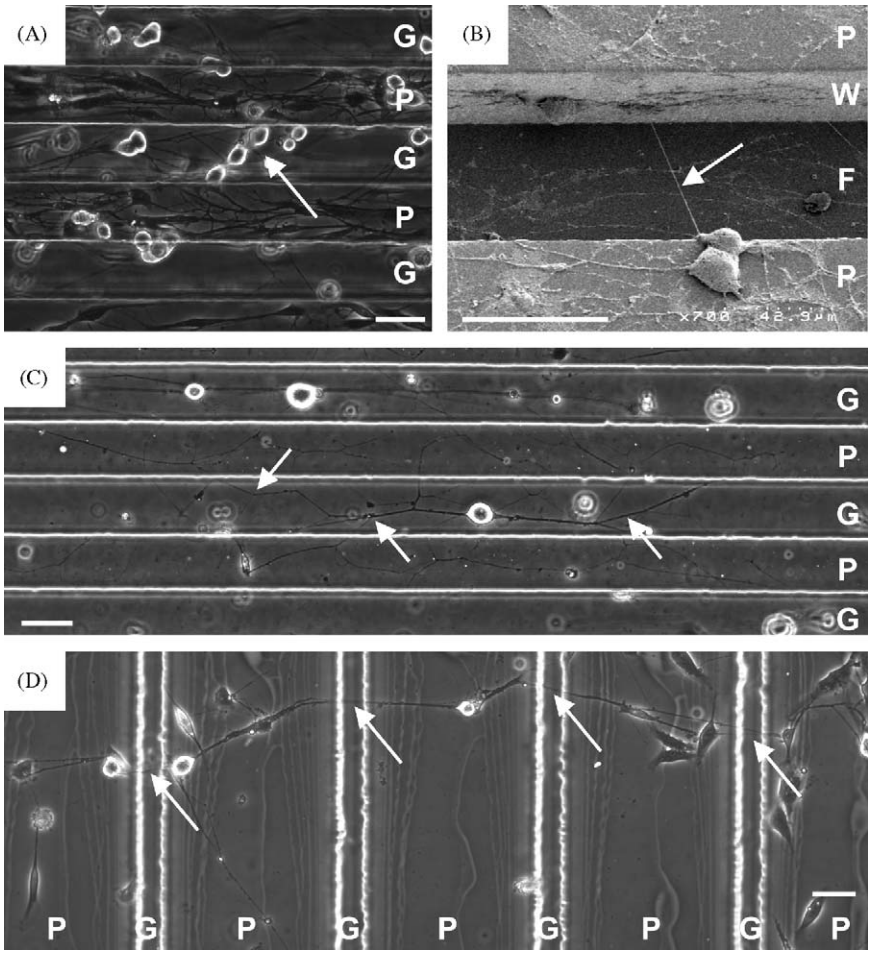

Fig. 3. Varied morphologies of DRG on micropatterned substrates: A. Phase contrast photomicrograph of DRG after 24 h culture on laminin-coated, micropatterned PDMS substrate with cell density of 125,000 cells/cm^2, w_g of 50 μm and w_p of 70 μm. An extensive network of neurites, including 3 somata that contact each other (arrow), is visible between two plateaus. B. Scanning electron micrograph of DRG after 24 h culture on laminin-coated, micropatterned PDMS substrate with cell density of 125,000 cells/cm^2, w_g of 50 μm and w_p of 70 μm. Arrow shows a neurite extending between a cell on the edge of the bottom plateau and a cell at mid-level of the groove wall. C. Phase contrast photomicrograph of DRG after 24 h culture on laminin-coated, micropatterned PDMS substrate with cell density of 12,500 cells/cm^2, w_g of 50 μm and w_p of 70 μm. Arrows show multiple bridging neurites from a single neuron suspended over a groove. D. Phase contrast photomicrograph of DRG after 3d culture on laminin-coated, micropatterned PDMS substrate with cell density of 12,500 cells/cm^2, w_g of 30 μm and w_p of 200 μm. Arrows show neurites bridging across four grooves. P, plateau; G, groove. Scale bars, 50 μm.

Fig. 2B. To facilitate the quantification experiments, we excluded from this counting any bridges that contained suspended somata, since they were more difficult to distinguish as individual bridges.

Cell density significantly influenced the numbers of neurite bridges ($p<0.001$, ANOVA). Minimal bridging was observed at 12,500 cells/cm^2, perhaps because the frequency of cell–cell interactions was too low to permit bridging or because, as the sample with the lowest cell density, it had fewer neurons from which to extend neurite bridges. Numbers of neurite bridges increased as cell concentration increased from 12,500 to 125,000, with highest numbers of neurite bridges observed at 125,000 cells/cm^2 (Fig. 5A). When normalized to cell concentration, numbers of neurite bridges per cell were highest for 62,500 and 125,000 cells/cm^2. Multiple comparison tests showed that seeding the substrate with 12,500 cells resulted in a significantly different number of neurite bridges from all other cell concentrations tested. Seeding the substrate with 62,500 cells resulted in a significantly different number of neurite bridges than seeding with 12,500 and 125,000 cells. These results are consistent with the notion that at the higher cell concentrations tested, cell–cell interactions within grooves or on plateaus predominate over cell–cell interactions that result in bridging between plateaus.

Groove width also significantly affected neurite bridges ($p<0.005$, ANOVA). Numbers of neurite bridges were highest at the lowest w_g tested: 30 μm (Fig. 5B). Above w_g of 100 μm, very few neurite bridges were observed, suggesting that beyond this threshold, the grooves were too wide for neurite bridging to occur

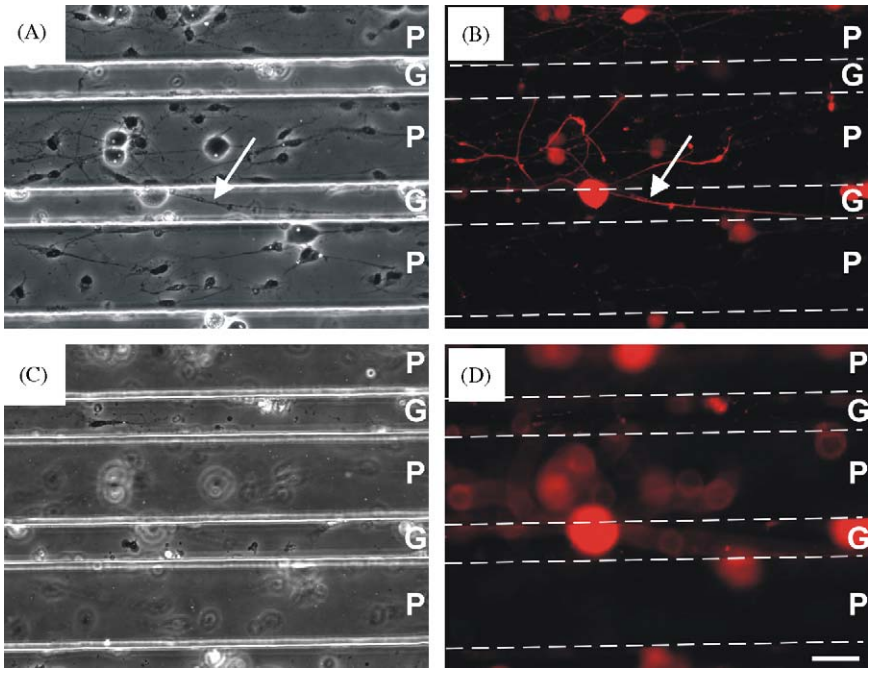

Fig. 4. DRG bridges are neurofilament-positive: Phase contrast (A, C) and epifluorescent (B, D) micrographs of DRG after 24 h culture on laminin-coated, micropatterned PDMS substrate with cell density of 125,000 cells/cm^2, w_g of 50 μm and w_p of 100 μm. All four images are of the same portion of the substrate. Immunofluorescent staining for neurofilament (B, D) shows a bridging neurite (arrow) visible in the plane of focus of the plateau (A, B), with no visible neurites in the plane of focus of the groove (C, D). The bridging neurite connects between a soma on one plateau and the ridge of the adjacent plateau, spanning across one groove. Dashed lines were added over the position of the groove walls in epifluorescent images to indicate the micropatterned features. P, plateau; G, groove. Scale bar, 50 μm.

at 24 h. A few atypical neurite bridges that were loosely attached to two plateaus were seen on substrates with 160 μm grooves and one neurite bridge has been observed spanning a groove of 200 μm. Post hoc multiple comparison tests showed that the number of neurite bridges found on the 30 μm grooved substrates differed significantly from those on the 200 and 1000 μm grooves, but not significantly from those on the 60, 130, or 160 μm grooves.

Further, we tested the effects of plateau width on neurite bridges, and found that plateau width affected neurite bridges significantly ($p<0.001$, ANOVA). The optimal w_p was 200 μm, with fewer neurite bridges observed from cells cultured on both narrower and wider plateaus (Fig. 5C). The numbers of neurite bridges on 200 μm plateau and on 1000 μm plateau substrates were significantly different from the numbers of neurite bridges on substrates with narrower (30 and 60 μm) plateaus.

A subpopulation of DRG exhibited neurite bridges on the grooved substrates, corresponding to approximately 1–3% of the total cell population. DRG contain multiple cell types, including neurons, fibroblasts, and glial cells. It is likely that the non-neuronal cells produced growth-promoting factors such as trophic factors and extracellular matrix molecules that contributed to the in vitro environment that was permissive for neurite extension. In addition, DRG neurons are comprised of several sensory neuron subpopulations that have been identified on the basis of anatomical, cytochemical, trophic, electrophysiological, and functional criteria [46–49]. Further studies will be needed to determine which subtype(s) of DRG neurons extend neurite bridges.

Preliminary studies in our laboratory have revealed effects of these topographically micropatterned substrates on process extension from other cell types. Bridging cellular extensions have been observed from cultures of embryonic rat hippocampal neurons (Fig. 6A–C), of adult rat Schwann cells (Fig. 6D–F), and of rat B104 neuroblastoma cells (Fig. 7A–B). It will be interesting in future work to investigate the range of cell types that exhibit the capacity to bridge micropatterned grooves with their cellular extensions.

3.4. Bridging and alignment

In these experiments the majority of DRG extended neurites parallel/aligning to the groove pattern, and a subset of DRG extended neurites perpendicular to/bridging the groove pattern. In previous studies, aligning and bridging neurites have been observed in response to grooved surfaces patterned at the nanometer—single micron scale. CNS neuroblasts have

been reported to migrate and orient their neurites both parallel and perpendicular to the axis of grooves with d_g on the order of 0.5 μm and w_g of 1 μm [39]. No bridging was observed at $w_g > 4$ μm. Embryonic rat hippocampal neurites have been shown to grow both parallel to grooves with d_g of 1 μm and w_g of 4 μm, and perpendicular to grooves with d_g of 130 nm and w_g of 1 μm [50]. The hippocampal neurites extended out of grooves and onto plateaus when d_g was 3.16 μm, and neurites were predicted to be unable to extend out of the grooves at $d_g \geqslant 4.7$ μm. The reported abilities of groove depth and groove width to constrain neurite extension out of grooves and onto adjacent plateaus contrast directly with the results of the present study, in which bridging neurites spanned grooves up to 100 μm wide and 50 μm deep. It is likely that the more narrow plateaus of the previous studies (1–8 μm vs. 30–1000 μm in the present study) provided a smaller surface area that was also more constraining and less favorable for neurite bridging.

Our observations of decreased bridging and corresponding increased alignment of neurites on substrates with more narrow plateaus agree with the results of Miller et al. [51], in which postnatal rat DRG neurons aligned with 10 μm plateaus more strongly than with 20 μm plateaus. This phenomenon has been described as a "flow effect" by which more narrow plateaus function to keep neurites aligned with the plateau-groove axis. Neurites in their study were also more likely to prefer laminin-coated grooves than uncoated plateaus, which may explain the lack of bridging neurites in their work, in contrast to the observations of the present study.

3.5. Dynamics of bridge formation

An unusual and surprising characteristic of the bridges observed in this study was that they had no underlying solid support; they spanned adjacent plateaus immersed in liquid media. Observation of neurons with SEM provided initial insight into a potential mechanism by which the bridges could form. In some instances neurites were observed extending between a cell soma on the floor of a groove and the groove wall

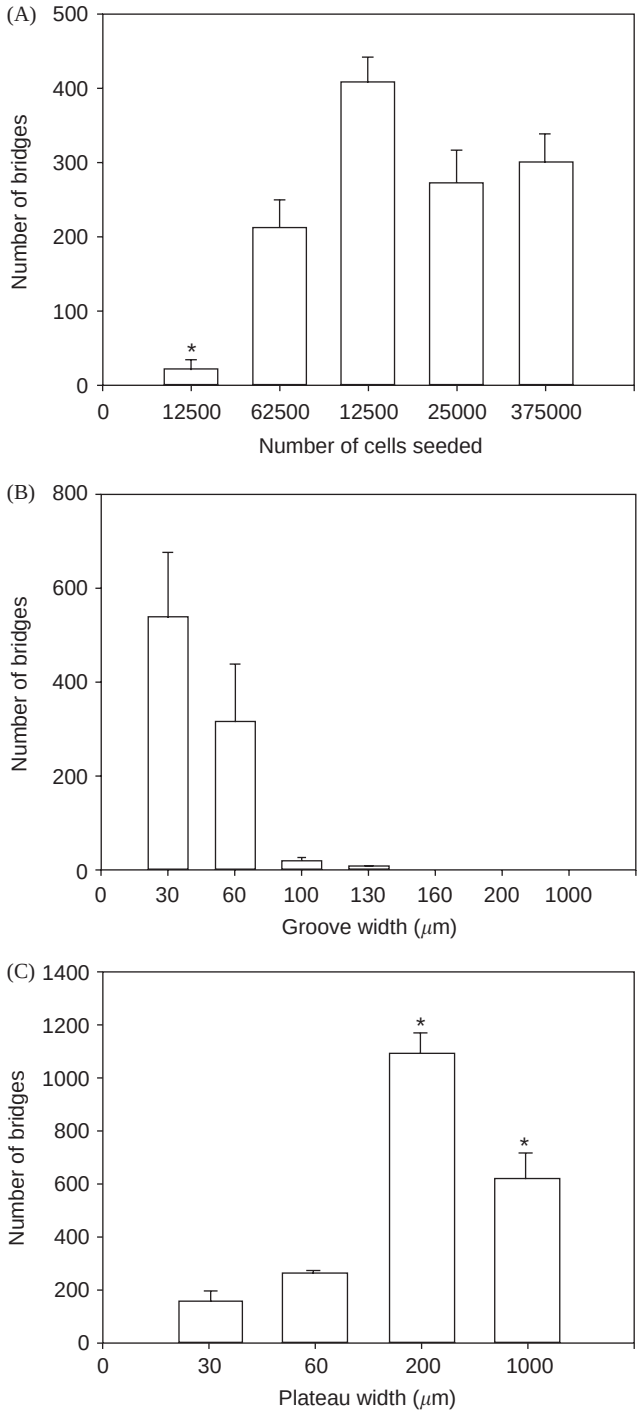

Fig. 5. A. Number of neurite bridges as a function of cell density: Mean number of neurite bridges per ten grooves[+] is shown for 5 cell densities tested. Substrate dimensions were d_g of 50 μm, w_g of 50 μm and w_p of 70 μm. The asterisk denotes the number of cells seeded that resulted in a significantly different number of neurite bridges when compared to all other cell densities tested. Seeding 125,000 cells resulted in the highest number of neurite bridges. ($n = 3$; error bars are SEM.) [+]The mean number of neurite bridges in 10 grooves for 375,000 cells was calculated from three samples. For one of these three, a projected value of neurite bridges in 10 grooves was used, since only six grooves could be counted due to an optical obstruction of a section of the PDMS substrate. B. Number of neurite bridges as a function of groove width: Mean number of neurite bridges per 10 grooves on substrates with varying groove widths. Experimental conditions were cell density of 125,000 cells per sample, d_g of 50 μm, and w_p of 100 μm. Grooves of 30 μm width resulted in significantly different numbers of neurite bridges than substrates with 200 and 1000 μm widths ($n = 4$ for $w_g = 30$, 60; $n = 3$ for $w_g = 200$, 1000; $n = 2$ for $w_g = 100$, 130, 160; error bars are SEM.) C. Number of neurite bridges as a function of plateau width: Mean number of neurite bridges per 10 grooves on substrates with varying plateau widths. Experimental conditions were cell density of 125,000 cells per sample, d_g of 50 μm, and w_g of 50 μm. Asterisks indicate the plateau widths that showed significantly different numbers of neurite bridges with respect to all other plateau widths tested. Highest number of neurite bridges was observed on substrates with plateau widths of 200 μm. ($n = 3$; error bars are SEM.)

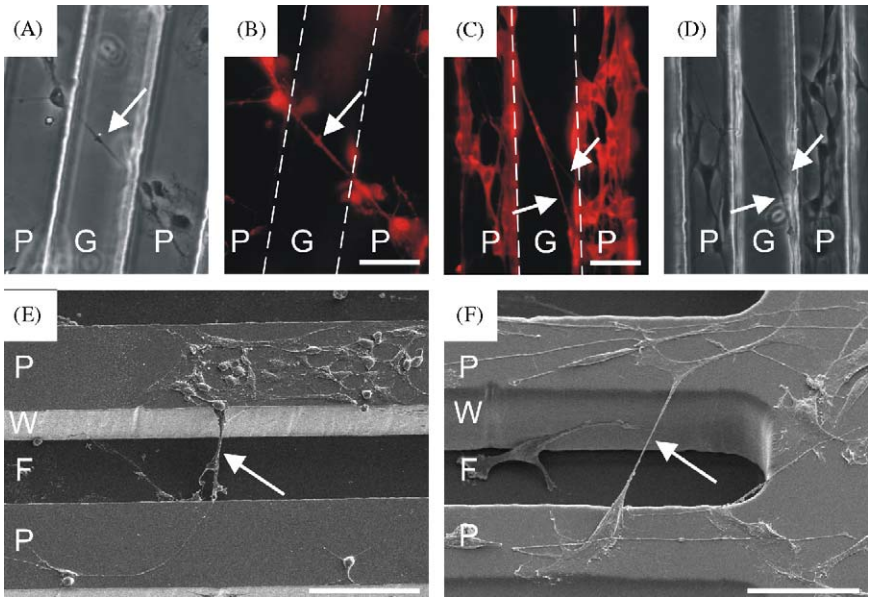

Fig. 6. Hippocampal neurons and Schwann cells extend bridges on micropatterned substrates: A-B. Phase contrast (A) and corresponding epifluorescent (B) photomicrographs of hippocampal neurons after 72 h culture on PLL-coated, micropatterned PDMS substrate with cell density of 50,000 cells/cm^2, w_g of 60 μm and w_p of 60 μm. Immunofluorescent staining for neurofilament shows a bridge that spans across the groove to connect two somata on adjacent plateaus. Dashed lines were added over the position of the groove walls in epifluorescent images to indicate the micropatterned features. Scale bar, 50 μm. C. Scanning electron micrograph of hippocampal neurons after 72 h culture on PLL-coated, micropatterned PDMS substrate with cell density of 50,000 cells/cm^2, w_g of 60 μm and w_p of 60 μm. Arrow shows a bridge that connects between a soma on the top plateau and a soma on the lower plateau (lower left corner of image). Scale bar, 66.7 μm. D-E. Phase contrast (D) and epifluorescent (E) photomicrographs of Schwann cells after 24 h culture on PLL-coated, micropatterned PDMS substrate with cell density of 50,000 cells/cm^2, w_g of 60 μm and w_p of 60 μm. Immunofluorescent staining for S100 protein shows Schwann cell processes (arrows) that connect between cells on the left plateau and cells on the right plateau, spanning across the groove in the form of a single process over the left groove region and two distinct processes over the right groove region. Dashed lines were added over the position of the groove walls in epifluorescent images to indicate the micropatterned features. Scale bar, 50 μm. F. Scanning electron micrograph of Schwann cell culture after 24 h culture on PLL-coated, micropatterned PDMS substrate with cell density of 50,000 cells/cm^2, w_g of 60 μm and w_p of 60 μm. Arrow shows a bridge spanning across a groove to connect cellular regions on adjacent plateaus. Scale bar, 60 μm. P, plateau; W, groove wall; F, groove floor.

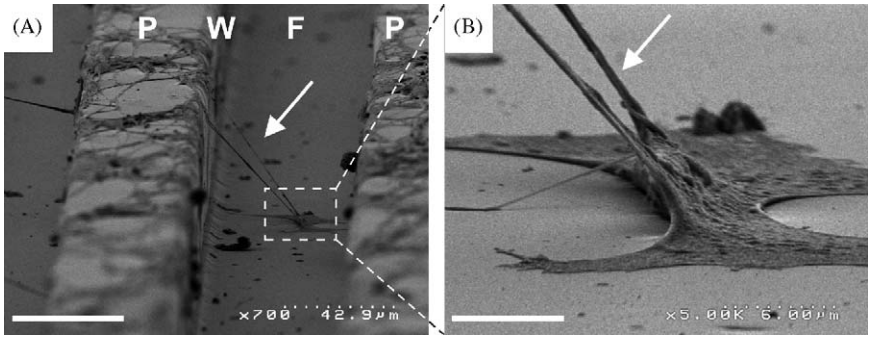

Fig. 7. Neuroblastoma bridges: A-B. Scanning electron micrographs of B104 rat neuroblastoma cells after 24 h culture on PLL-coated, micropatterned PDMS substrate with cell density of 50,000 cells/cm^2, w_g of 60 μm and w_p of 60 μm. A. Arrow shows two neurites connecting a cell on the groove floor to the top edge of the groove wall. Scale bar, 42.9 μm. B. Close-up view of cell in panel A, showing two neurites directed upwards with part of the soma rising off the groove floor, and one smaller neurite directed downwards and adhering to the groove floor. Scale bar, 6 μm.

(Fig. 7A, B). In the region of the cell where the neurites emerged from the cell soma, part of the soma was lifted off the substrate. We hypothesized that this lifting was an early event in the formation of a bridge, and we carried out studies using time-lapse microscopy in order to characterize the dynamics of bridge formation.

We observed DRG neurons cultured on micropatterned substrates during the period of 3–24 h after plating, and analyzed the formation of 11 bridges. Cultures were highly dynamic, with cell migration and process extension and retraction throughout the time of observation (see movies in supplemental data). When a

bridge was observed, its presence was preceded by the series of events depicted in Fig. 8A. At time $t1$, a cell that has adhered to the floor of a groove extends neurites on the groove floor. At $t2$, the neurites extend partway up the groove walls, then extend higher toward the adjacent plateaus during $t3$–$t4$. As the neurites extend higher, the cell body detaches from the groove floor and rises toward the level of the plateaus. At $t5$, the cell body and neurites are suspended over the groove, bridging across the two adjacent plateaus. The cell body then translocates to one of the adjacent plateaus where it is shown at $t6$.

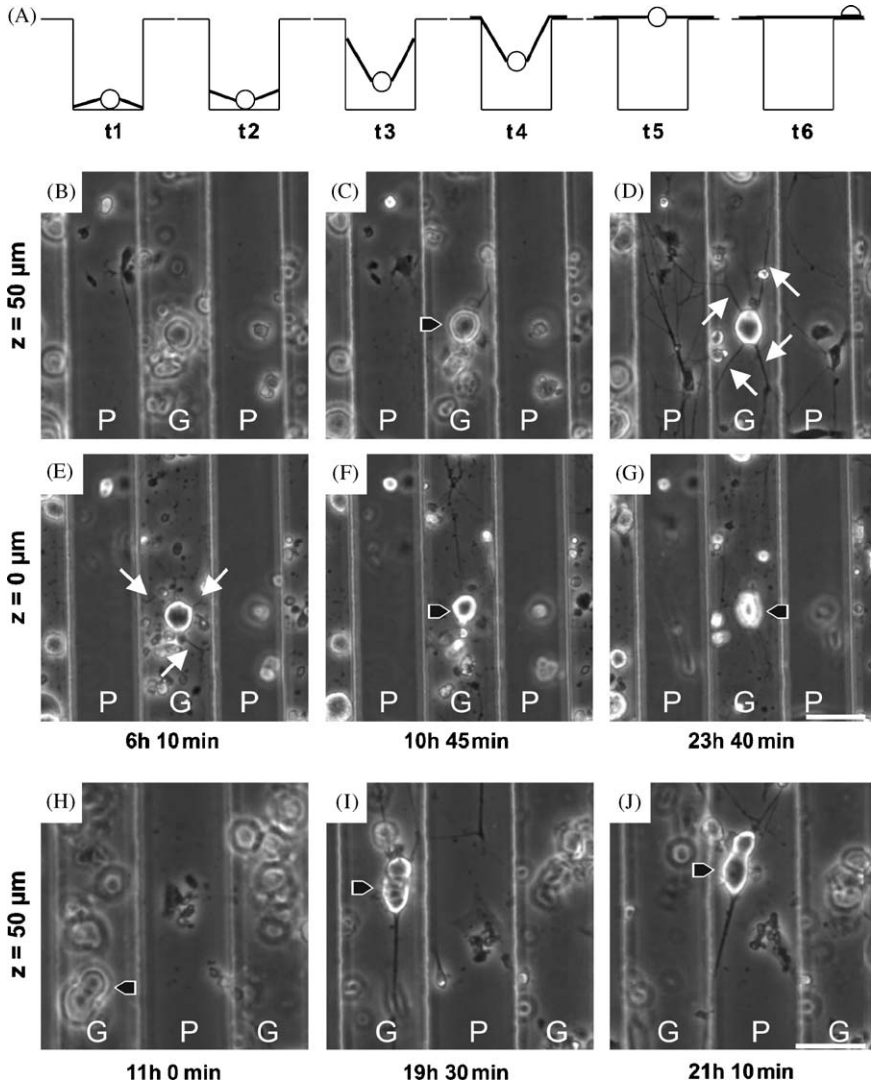

Fig. 8. Dynamics of bridge formation: A. Cartoon depicts representative cell growth on a micropatterned substrate over time. The substrate is shown from the side, looking down the length of a groove at a cell extending processes. From time $t1$ to time $t5$, the processes extend up the groove walls to the plateau surfaces, and the cell body moves from its initial position, adhered to the groove floor, to become suspended over the groove, with processes bridging between adjacent plateaus. From time $t5$ to time $t6$, the cell body moves laterally to adhere to the adjacent plateau. B–J. Phase contrast micrographs obtained by time-lapse microscopy showing the dynamics of bridge formation from DRG cultured on laminin-coated, micropatterned PDMS substrate with cell density of 100,000 cells/cm^2, w_g of 60 µm and w_p of 60 µm. The events underlying bridge formation from two distinct neurons are shown (B–G and H–J). For the first neuron, micrographs of a single substrate region of 207 µm width by 207 µm length are shown at the planes of focus of the plateau (B–D; $z = 50$ µm) and of the groove floor (E–G; $z = 0$ µm), at three time points during 6–24 h after plating. Note that at 6 h 10 min the soma and neurites were in focus on the groove floor (E) but not at the level of the plateau (B). This time point corresponds to $t1$ (A). At 10 h 45 min, the soma and neurites were visible but out of focus when viewed at the plateau level (C) and at the floor level (F), corresponding to $t3$ (A). At 23 h 40 min, the soma and neurites were in focus at the plateau (D) and not at the groove (G), corresponding to $t5$ (A). For the second neuron, micrographs of a single substrate region of 207 µm width by 207 µm length are shown at the plane of focus of the plateau (H–J; $z = 50$ µm), at three time points during 11–22 h after plating. Note that at 11 h the soma and neurite were on the groove floor and therefore out of focus at the level of the plateau (H), corresponding to $t2$ (A). At 19 h 30 min, the soma and neurite were in focus over the groove, at the plane of focus of the plateau (I), corresponding to $t5$ (A). By 21 h 10 min, the soma and neurite were visible and in focus on the plateau (J), corresponding to $t6$(A). White arrows, neurites; black arrowheads, somata; P, plateau; G, groove. Scale bars, 50 µm.

Representative images of this process are shown for two cultures in Fig. 8 with views at the focus plane of the plateau (8B–D, 8H–J) and at the focus plane of the groove (8E–G). In the first case (8B–G), at 6 h 10 min, neurites from a cell on the groove floor extended toward the groove wall with lengths of 17–32 μm (arrows in 8E), and the cell was out of focus at the level of the plateau (8B). At 10 h 45 min, neurites moved toward the top of the plateau while contacting the groove wall, and the soma began to lift off of the groove floor. At this point the soma and neurites were out of focus in both the groove floor and plateau focus planes (arrow heads in 8C and F). The neuron slowly rose upward until the soma was suspended by four neurites at the level of the plateau after 23 h 40 min (arrows in 8D). The lengths of the neurite regions that were suspended over the groove were 34–93 μm. The neuron was suspended in media as illustrated by the lack of neurites on the groove floor (8G). The images at these three time points approximate the conditions at $t1$, $t3$, and $t5$ as depicted in Fig. 8a.

In the second case (8H–J), at 11 h two neurons and their extended neurites were present on the groove floor and therefore out of focus at the focus plane of the plateau (8H). The neurons rose upwards until they were suspended by three neurites at the level of the plateau after 19 h 30 min (8I). The lengths of the neurite regions that were suspended over the groove were between 24 μm and at least 244 μm (the attachment point for the longest neurite was out of the field of view by 19 h 30 min). The somata then translocated to the right onto the adjacent plateau, as clearly visible at 21 h 10 min (8J). At this point a neurite extended between the somata on one plateau and the surface of the adjacent plateau, with a suspended neurite bridge spanning the groove between the two plateaus (neurite out of the field of view of 8J). The images at these three time points approximate the conditions at $t2$, $t5$, and $t6$ as depicted in Fig. 8A.

We hypothesize that bridging occurs when neurons exert forces on each other that can override the effects of substrate features on neurite alignment, as has been suggested previously in studies of the effects of micro-topography on fibroblasts [33]. As fibroblasts respond to topography, the actin cytoskeleton has been shown to be important [21]; however, in the case of neurite guidance by topographical features, treatment with actin and tubulin inhibitors did not disrupt the neurite preference for grooves. In contrast, calcium influx by voltage-dependent calcium channels and protein kinase C have been suggested to be involved in neurite guidance in response to grooved topography [52]. Physical tension has also been shown to influence neurite extension, as demonstrated by Chada et al. [53]. Further studies including pharmacological experiments will be needed to elucidate the cytoskeletal mechanisms that underlie the bridging phemonenon observed in the present study.

4. Conclusions

A major finding of this study is that postnatal rat DRG neurons exhibit complex interactions with micro-patterned substrates that contain topographical features of dimensions from tens to hundreds of microns. When cultured on micropatterned substrates, a population of neurons demonstrated a unique growth pattern, with neurites bridging across grooves between adjacent plateaus. The dynamic growth of these neurites—pulling a neuron 50 μm above its initial adhesion point to suspend it between grooves in the absence of underlying solid support—is particularly interesting in the context of understanding the intracellular mechanisms that mediate neurite extension and axon guidance.

Efforts to promote nerve regeneration must consider that axons attempting to regrow after an injury navigate a complex, 3D matrix of molecules and cells. A more rigorous comprehension of how neurons respond to 3D topographical cues is critical as scientists apply micro-fabrication technologies such as those used in the present study, in efforts to guide axons. Significantly, strategies for axon guidance that employ grooved substrates to align and direct neurons and glial cells must take into account the results demonstrated here: that neurons and glia have the capacity to grow counter to the intended direction of growth. The results from this study can influence the design of future tissue engineering scaffolds that tailor topographical features (i.e. pores) to optimize cell-scaffold interactions, in order to incorporate and sustain cells to support nerve regeneration.

Acknowledgements

The authors thank Michael Angelo Santos and Leigh Needleman for assistance with cell cultures and Pearl Yu for assistance with manuscript preparation. This work was funded by grants from NSF (REU fellowship to J.S.G.) and the Whitaker Foundation.

Appendix A. Supplemental data

Figs. S1 and S2 contain two movies of sequential phase contrast micrographs obtained by timelapse microscopy showing the dynamics of bridge formation from DRG cultured on laminin coated, micropatterned PDMS substrate with cell density of 100,000 cells/cm^2, w_g of 60 μm and w_p of 60 μm. Movies of a single substrate region of 225 μm width by 229 μm length are shown at the planes of focus of the groove floor (S1) and of the plateau (S2) over 248 time points, five minutes apart, starting 3 h after plating. The frame rate of the movie is 6 frames/s, corresponding to 30 min of elapsed

real time per second of movie. The neuron of interest is the neuron present in Fig. 8B–G.

Supplementary data associated with this article can be found in the online version at doi:10.1016/j.biomaterials.2005.06.035.

References

[1] Schwab ME, Thoenen H. Dissociated neurons regenerate into sciatic but not optic nerve explants in culture irrespective of neurotrophic factors. J Neurosci 1985;5(9):2415–23.

[2] Caroni P, Schwab ME. Two membrane protein fractions from rat central myelin with inhibitory properties for neurite growth and fibroblast spreading. J Cell Biol 1988;106(4):1281–8.

[3] Schwab ME, Kapfhammer JP, Bandtlow CE. Inhibotors of neurite outgrowth. Ann Rev Neurosci 1993;16:565–95.

[4] McKeon RJ, Schreiber RC, Rudge JS, Silver J. Reduction of neurite outgrowth in a model of glial scarring following CNS injury is correlated with the expression of inhibitory molecules on reactive astrocytes. J Neuroscience 1991;11(11):3398–411.

[5] Fawcett JW, Asher RA. The glial scar and central nervous system repair. Brain Res Bull 1999;49(6):377–91.

[6] Reier PJ, Houle JD. The glial scar: its bearing on axonal elongation and transplantation approaches to CNS repair. Adv Neurol 1988;47:87–138.

[7] Aguayo AJ, David S, Bray GM. Influences of the glial environment on the elongation of axons after injury: transplantation studies in adult rodents. J Exp Biol 1981;95:231–40.

[8] Bray GM, Vidal-Sanz M, Aguayo AJ. Regeneration of axons from the central nervous system of adult rats. Prog Brain Res 1987;71:373–9.

[9] Richardson PM. Neurotrophic factors in regeneration. Curr Opin Neurobiol 1991;1(3):401–6.

[10] Hynes RO, Lander AD. Contact and adhesive specificities in the associations, migrations, and targeting of cells and axons. Cell 1992;68(2):303–22.

[11] McCaig CD, Rajnicek AM. Electrical fields, nerve growth and nerve regeneration. Exp Physiol 1991;76:473–94.

[12] Newgreen DF. Physical influences on neural crest migration in avian embryos: contact guidance and spatial restriction. Dev Biol 1989;131:136–48.

[13] Nagata I, Nakatsuji N. Rodent CNS neuroblasts exhibit both perpendicular and parallel contact guidance on the aligned parallel neurite bundle. Development 1991;112:581–90.

[14] Ebendal T, Jacobson CO. Tissue explants affecting extension and orientation of axons in cultured chick embryo ganglia. Exp Cell Res 1977;105(2):379–87.

[15] Lofberg J, Ebendal T. Substrate topography and shape of motile cells. Experientia 1980;36(5):508–10.

[16] Ito Y. Surface micropatterning to regulate cell functions. Biomaterials 1999;20:2333–42.

[17] Curtis A, Wilkinson C. Topographical control of cells. Biomaterials 1997;18:1573–83.

[18] Curtis ASG, Varde M. Control of cell behavior: topographical factors. J Natl Cancer Res Inst 1964;33:15–26.

[19] Dunn GA, Heath JP. A new hypothesis of contact guidance in tissue cells. Exp Cell Res 1976;101:1–14.

[20] Ohara PT, Buck RC. Contact guidance in vitro. A light, transmission, and scanning electron microscopic study. Exp Cell Res 1979;121:235–49.

[21] Wojciak-Stothard B, Curtis ASG, Monaghan W, McGrath M, Sommer I, Wilkinson CDW. Role of the cytoskeleton in the reaction of fibroblasts to multiple grooved substrata. Cell Motil Cytoskeleton 1995;31:147–58.

[22] Flemming RG, Murphy CJ, Abrams GA, Goodman SL, Nealy PF. Effects of synthetic micro- and nano-structured surfaces on cell behavior. Biomaterials 1999;20:573–88.

[23] Clark P, Connolly P, Curtis ASG, Dow JAT, Wilkinson CDW. Topographical control of cell behaviour I. Simple step cues. Development 1987;99:439–48.

[24] Bruinink A, Wintermantel E. Grooves affect primary bone marrow but not osteoblastic MC3T3-E1 cell cultures. Biomaterials 2001;22:2465–73.

[25] Clark P, Connolly P, Curtis ASG, Dow JAT, Wilkinson CDW. Cell guidance by ultrafine topography in vitro. J Cell Sci 1991;99:73–7.

[26] Wojciak-Stothard B, Madeja Z, Korohoda W, Curtis A, Wilkinson C. Activation of macrophage-like cells by multiple grooved substrata. Topographical control of cell behaviour. Cell Biol Int 1995;19:485–90.

[27] Webster TJ, Ergun C, Doremus RH, Siegel RW, Bizios R. Enhanced osteoclast-like cell functions on nanophase ceramics. Biomaterials 2001;22:1327–33.

[28] Eisenbarth E, Meyle J, Nachtigall W, Breme J. Influence of the surface structure of titanium materials on the adhesion of fibroblasts. Biomaterials 1996;17:1399–403.

[29] Eriksson C, Lausmaa J, Nygren H. Interactions between human whole blood and modified Ti–O_2-surfaces: influence of surface topography and oxide thickness on leukocyte adhesion and activation. Biomaterials 2001;22:1987–96.

[30] Dalby MJ, Kayser MV, Bonfield W, Di Silvio L. Initial interaction of osteoblasts to an optimised HAPEX^{TM} topography. Biomaterials 2002;23:681–90.

[31] Curtis ASG, Casey B, Gallagher JO, Pasqui D, Wood MA, Wilkinson CDW. Substratum nanotopgraphy and the adhesion of biological cells. Are symmetry or regularity of nanotopography important? Biophys Chem 2001;94:275–83.

[32] Miller CA, Shanks H, Witt A, Rutkowski G, Mallapragada SK. Oriented schwann cell growth on micropatterned biodegradable polymer substrates. Biomaterials 2001;22:1263–9.

[33] Clark P, Connolly P, Curtis ASG, Dow JAT, Wilkinson CDW. Topographical control of cell behaviour: II. multiple grooved substrata. Development 1990;108:635–44.

[34] Brunette DM. Fibroblasts on micromachined substrata orient hierarchically to grooves of different dimensions. Exp Cell Res 1986;164:11.

[35] Hirono T, Torimitsu K, Kawana A, Fukuda J. Recognition of artificial microstructures by sensory nerve fibers in culture. Brain Res 1988;446:189–94.

[36] Folch A, Toner M. Microengineering of cellular interactions. Ann Rev Biomed Eng 2000;2:227–56.

[37] Connolly P. Bioelectronic interfacing: micro- and nanofabrication techniques for generating predetermined molecular arrays. Trends Biotechnol 1994;12(4):123–7.

[38] Wilkinson CDW, Curtis ASG, Crossan J. Nanofabrication in cellular engineering. J Vac Sci Technol 1998;B 16:3132–6.

[39] Nagata I, Kawana A, Nakatsuji N. Perpendicular contact guidance of CNS neuroblasts on artificial microstructures. Development 1993;117:401–8.

[40] Rajnicek A, Britland S, McCaig C. Contact guidance of CNS neurites on grooved quartz: influence of groove dimensions, neuronal age and cell type. J Cell Sci 1997;110(Pt 23):2905–13.

[41] Morrissey TK, Kleitman N, Bunge RP. Isolation and functional characterization of Schwann cells derived from adult peripheral nerve. J Neurosci 1991;11(8):2433–42.

[42] Luckenbill-Edds L. Laminin and the mechanism of neuronal outgrowth. Brain Res Brain Res Rev 1997;23(1–2):1–27.

[43] Madison RD, da Silva C, Dikkes P, Sidman RL, Chiu TH. Peripheral nerve regeneration with entubulation repair: comparison of biodegradeable nerve guides versus polyethylene tubes and

the effects of a laminin-containing gel. Exp Neurol 1987;95(2): 378–90.
[44] Martini R. Expression and functional roles of neural cell surface molecules and extracellular matrix components during development and regeneration of peripheral nerves. J Neurocytol 1994; 23(1):1–28.
[45] Grimpe B, Dong S, Doller C, Temple K, Malouf AT, Silver J. The critical role of basement membrane-independent laminin gamma 1 chain during axon regeneration in the CNS. J Neurosci 2002;22(8):3144–60.
[46] Perl ER. Function of dorsal root ganglion neurons: an overview. New York: Oxford UP; 1992.
[47] McMahon S, Armanini M, Ling L, Phillips H. Expression and coexpression of Trk receptors in subpopulations of adult primary sensory neurons projecting to identified peripheral targets. Neuron 1994;12:1161–71.
[48] Gilabert R, McNaugthon P. Enrichment of the fraction of nociceptive neurons in cultures of primary sensory neurons. J Neurosci Methods 1997;71:191–8.
[49] Baudet C, Mikarls A, Westphal H, Johansen J, Johansen T, Ernfors P. Positive and negative interactions of GDNF, NTN, ART in developing sensory neuron subpopulations, and their collaboration with neurotrophin. Development 2000;127: 4335–44.
[50] Rajnicek AM, Britland S, McCaig CD. Contact guidance of CNS neurites on grooved quartz: influence of groove dimensions, neuronal age and cell type. J Cell Sci 1997;110:2905–13.
[51] Miller C, Jeftinija S, Mallapragada S. Synergistic effects of physical and chemical guidance cues on neurite alignment and outgrowth on biodegradable polymer substrates. Tissue Eng 2002;8(3):367–78.
[52] Rajnicek AM, McCaig CD. Guidance of CNS growth cones by substratum grooves and ridges: effects of inhibitors of the cytoskeleton, calcium channels and signal transduction pathways. J Cell Sci 1997;110:2915–24.
[53] Chada S, Lamoureux P, Buxbaum RE, Heidemann SR. Cytomechanics of neurite outgrowth from chick brain neurons. J Cell Sci 1997;110:1179–86.